High-Kinetic-Inductance Superconducting Nanowire Resonators for Circuit QED in a Magnetic Field

Samkharadze, N.; Bruno, A.; Scarlino, P.; Zheng, G.; Divincenzo, D.P.; DiCarlo, L.; Vandersypen, L. M K

DOI
10.1103/PhysRevApplied.5.044004

Publication date
2016

Document Version
Final published version

Published in
Physical Review Applied

Citation (APA)
Samkharadze, N., Bruno, A., Scarlino, P., Zheng, G., Divincenzo, D. P., DiCarlo, L., & Vandersypen, L. M. K. (2016). High-Kinetic-Inductance Superconducting Nanowire Resonators for Circuit QED in a Magnetic Field. *Physical Review Applied*, *5*(4), [044004]. https://doi.org/10.1103/PhysRevApplied.5.044004

PHYSICAL REVIEW APPLIED **5,** 044004 (2016)

High-Kinetic-Inductance Superconducting Nanowire Resonators for Circuit QED in a Magnetic Field

N. Samkharadze,[1] A. Bruno,[1] P. Scarlino,[1] G. Zheng,[1] D. P. DiVincenzo,[2] L. DiCarlo,[1] and L. M. K. Vandersypen[1]
[1]*QuTech and Kavli Institute of Nanoscience, Delft University of Technology,*
Lorentzweg 1, 2628 CJ Delft, The Netherlands
[2]*JARA Institute for Quantum Information, RWTH Aachen University, D-52056 Aachen, Germany*

(Received 4 November 2015; revised manuscript received 12 February 2016; published 7 April 2016)

We present superconducting microwave-frequency resonators based on NbTiN nanowires. The small cross section of the nanowires minimizes vortex generation, making the resonators resilient to magnetic fields. Measured intrinsic quality factors exceed 2×10^5 in a 6-T in-plane magnetic field and 3×10^4 in a 350-mT perpendicular magnetic field. Because of their high characteristic impedance, these resonators are expected to develop zero-point voltage fluctuations one order of magnitude larger than in standard coplanar waveguide resonators. These properties make the nanowire resonators well suited for circuit QED experiments needing strong coupling to quantum systems with small electric dipole moments and requiring a magnetic field, such as electrons in single and double quantum dots.

DOI: 10.1103/PhysRevApplied.5.044004

I. INTRODUCTION

Superconducting microwave-frequency resonators are widely considered essential building blocks of future quantum processors, providing a means for qubit readout and long-range interconnect in a circuit quantum electrodynamics (cQED) architecture [1]. They also offer a promising interface between different types of quantum systems [2]. To reap the full benefits of cQED architectures, it is crucial to reach the strong-coupling regime, wherein quantum-state transfer between the qubit and the resonator is possible on a time scale shorter than the coherence time of the combined system.

Several proposals have been put forward for implementing cQED using electron-spin qubits in semiconducting quantum dots [3–7]. Electron spins offer very long coherence times, in some case of order a second [8–10], but convincing mechanisms for scaling in 2D are still lacking. Therefore, exploring cQED as a means for scaling is of high importance. Pioneering experiments have demonstrated coupling of superconducting cavity modes with spin and orbital degrees of freedom of the electrons [11–14].

Achieving strong coupling in such hybrid systems has proved challenging due to the weak interaction between the zero-point fluctuations (ZPFs) of conventional superconducting resonators and the quantum-dot electrons. Traditionally, coplanar waveguide (CPW) resonators with characteristic impedance $Z_r \sim 50\ \Omega$ have been used as the staple cavity in cQED. However, by increasing (decreasing) Z_r, it is possible to enhance the ZPFs of voltage (current), thus, optimizing for electric (magnetic) dipole coupling to qubits.

Another challenge in incorporating superconducting resonators in spin- or Majorana-based systems is the typically poor performance of superconducting resonators at the magnetic fields required for the operation of such systems. Intrinsic quality factors $Q_i > 10^6$ have been measured for the highest-performance resonators in magnetically shielded cQED setups [15,16]. However, strong magnetic fields induce vortices in the superconducting film, which move under the influence of microwave currents in the resonator, causing energy dissipation. A few methods have been employed to minimize vortex-induced dissipation in superconducting devices. These methods include creating artificial pinning sites and dams for the vortices [17–20] and steering the vortices away from the areas carrying the highest currents [17,21–23]. To date, the most effective magnetic field resilience has been achieved in superconducting fractal resonators, with $Q_i \approx 10^5$ in a parallel magnetic field $B_{\parallel} \approx 400$ mT [22,23], and more recently, in YBCO CPW resonators with $Q_i \approx 2 \times 10^4$ at $B_{\parallel} = 7$ T [24].

In this article, we present microwave-frequency resonators based on NbTiN nanowires, displaying magnetic field resilience and promising stronger electrical coupling. We take advantage of the high kinetic inductance of the strongly disordered superconducting nanowires to increase $Z_r = \sqrt{\mathcal{L}/\mathcal{C}}$ and thereby also the voltage ZPFs, $V_{\mathrm{rms}}^{\mathrm{ZPF}} \propto f_r\sqrt{Z_r}$ [25,26]. Here, f_r is the resonance frequency, and $\mathcal{L}$ ($\mathcal{C}$) is the inductance (capacitance) per unit length of the nanowire. We estimate $Z_r \approx 4\ \mathrm{k}\Omega$, nearly 2 orders of magnitude higher than that of CPW resonators used in typical cQED devices. The corresponding $V_{\mathrm{rms}}^{\mathrm{ZPF}} \sim 20\ \mu$V makes these resonators well suited for coupling to systems with small electric dipole moments, such as electrons in single or double quantum dots. Moreover, the small nanowire cross section strongly suppresses vortex generation in a magnetic field, resulting in $Q_i > 2 \times 10^5$ up to $B_{\parallel} = 6$ T. We also investigate the evolution of these resonators with perpendicular magnetic field $B_{\perp}$, finding a clear dependence of the magnetic field resilience of Q_i on the nanowire width w. The narrowest nanowires ($w \approx 100$ nm) achieve $Q_i > 3 \times 10^4$ at $B_{\perp} \approx 350$ mT.

II. METHODS

The resonators consist of NbTiN nanowire loops interrupted by a small gap (Fig. 1) and coupled to a common CPW feedline. To minimize $\mathcal{C}$, the nanowire is detracted as far as possible from the ground planes, with the distance being limited by the requirement of sufficient coupling strength to the feedline. Figure 1(d) shows the simulated feedline transmission for the device shown in Fig. 1(a). The ratio between the resonance frequencies of the two lowest modes extracted from the simulation is 2.01, demonstrating that the nanowire resonators are essentially distributed resonators with a negligible direct capacitance between the nanowire ends. In the configuration of Fig. 1(a), the coupling of the fundamental (half-wave) mode of the resonator to the feedline is inductive, which for our high impedance resonators is extremely weak [Fig. 1(a)]; therefore, we focus on the full-wave mode, leaving the discussion of the fundamental to Appendix A.

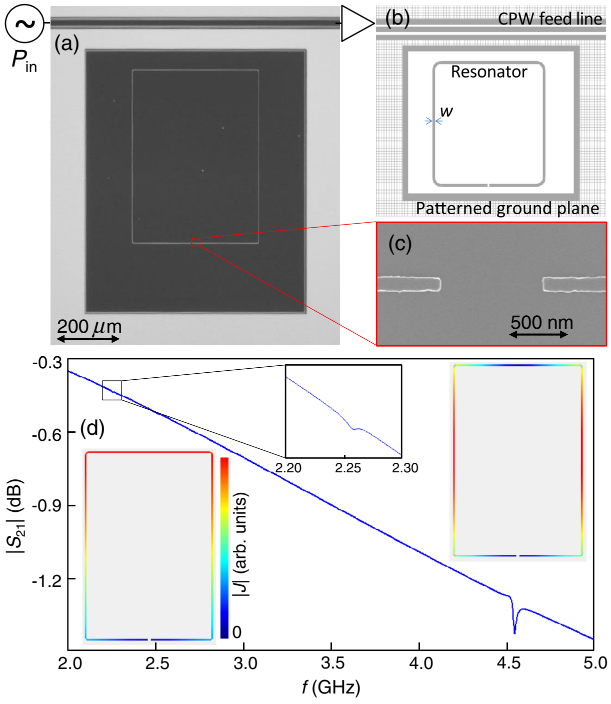

FIG. 1. Resonator design. (a) Dark-field optical image of a typical nanowire resonator. (b) Schematic (not to scale) showing the nanowire resonator, CPW feedline, and patterned ground plane. Here, NbTiN is shown in gray and Si substrate is white. The ground plane is patterned in a square grid shape to enhance the visibility for wire bonding. We see no evidence of ground plane patterning affecting performance of the resonators in the magnetic field. (c) Scanning-electron-microscope enlargement of the gap of a typical resonator. (d) Simulated feedline transmission for the device in (a). The insets show (absolute) current distributions along the nanowire for the fundamental and second resonance modes, as well as an enlargement of the feedline transmission near the fundamental resonance.

Device fabrication begins with sputtering of a NbTiN film (thickness $t \sim 8$ nm) on a high-resistivity Si⟨100⟩ substrate [16,27]. A CPW feedline and several (four or five) nanowire resonators are next defined in a single electron-beam lithography step followed by reactive ion etching in a SF_6/He plasma. The completed devices are cooled in a ^{3}He refrigerator with 280-mK base temperature and 70-dB cold attenuation between room temperature and the feedline input. Each resonator is characterized by measuring the complex-valued feedline transmission near its resonance (Fig. 2). A fitting of the model from Ref. [25] to the data allows us to extract the resonance frequency and the coupling and intrinsic quality factors [16,28]. Each resonator is designed to have the coupling quality factor $Q_C \approx 10^5$, the same order of magnitude as the intrinsic quality factor.

The highly disordered nature of NbTiN and the extremely small cross-sectional area of the nanowires make

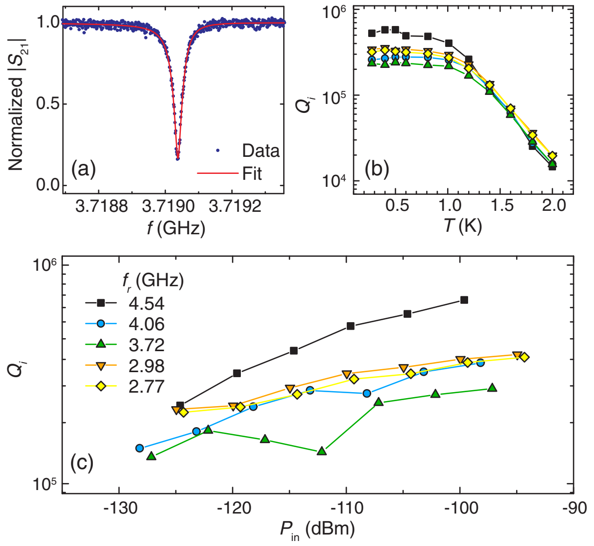

FIG. 2. Power and temperature dependence of intrinsic quality factors of five nanowire resonators. (a) Normalized absolute transmission around a typical resonance. The curve is constructed from the best fit to the complex-valued feedline transmission data [16,28]. (b) Temperature dependence of intrinsic quality factors measured at a fixed input power $P_{in} \approx -110$ dBm. The symbols correspond to the legend in (c). Two distinct regimes are observed for $T < 1$ K and $T > 1$ K, in which dominant loss is expected from TLS and quasiparticle dissipation, respectively. (c) Power dependence of intrinsic quality factors measured at 280 mK. The positive slope is consistent with TLS-dominated loss.

the kinetic inductance the dominant contribution to the total inductance of the resonators. From the measured critical temperature $T_c \approx 9.3$ K and room-temperature resistivity $\rho = 200\ \mu\Omega$ cm of the film, we estimate a sheet kinetic inductance $L_S \approx 35$ pH/□ [29], close to the value 38 pH/□ needed in a Sonnet simulation to match the resonance in Fig. 1(d) to the measurements. For a resonator of length $l = 2.9$ mm and $w = 100$ nm (2.77-GHz full-wave mode), this corresponds to a total in-line inductance $\mathcal{L}l \sim 1\ \mu$H.

III. RESULTS AND DISCUSSION

Figure 2(c) shows Q_i of five resonators ($w = 100$ nm) as a function of input power, P_{in}. We find $Q_i > 10^5$ at $P_{\mathrm{in}} \approx -130$ dBm corresponding to an average occupation of the resonator by $\langle n_{\mathrm{ph}} \rangle \approx 10$ photons. The observed increase of Q_i with P_{in} indicates dominant loss by coupling to spurious two-level systems (TLSs) which saturate at high power [16,30,31]. This conclusion is further supported by the temperature dependence of Q_i at $P_{\mathrm{in}} \approx -110$ dBm, corresponding to $\langle n_{\mathrm{ph}} \rangle \approx 1000$ [Fig. 2(b)]. Thermally excited quasiparticles dominate loss only above 1 K $\sim T_c/10$, consistent with previous studies of quasiparticle-induced dissipation in highly disordered thin-film resonators [32].

A. Performance of the resonators in a magnetic field

The resilience of the nanowire resonators to a magnetic field is seen in Fig. 3, which shows the typical dependence of intrinsic quality factors on the applied $B_\parallel$. Most strikingly, for $B_\parallel$ between 400 mT and 6 T, Q_i is consistently above 10^5 without sign of degradation. This field is at least one order of magnitude higher than the highest at which such Q_i has been reported in earlier studies of planar superconducting resonators [22,23]. Moreover, we do not observe hysteretic behavior or abrupt jumps in f_r with increasing $B_\parallel$. These effects plague standard CPW resonators and are usually attributed to unstable magnetic-flux vortices in the superconducting film [19,22,33,34]. These findings suggest that vortex nucleation does not take place in the nanowires. Vortices may still be created in the ground plane. However, due to the large separation between the nanowires and the ground planes, we expect only minimal current densities to be induced in the ground plane, thus, weakly contributing to dissipation.

Further insight into the effect of a magnetic field on the resonators is gained by orienting the field perpendicular to the device plane. Figure 4(a) shows the dependence of Q_i in seven nanowire resonators (widths ranging from $w = 100$ to 700 nm) on $B_\perp$. The magnetic field resilience depends strongly on the nanowire width, and the narrowest resonators show superior performance. We observe $Q_i > 3 \times 10^4$ for the narrowest resonator ($w = 100$ nm) for $B_\perp \le 350$ mT [Fig. 4(a)]. This field range is one order

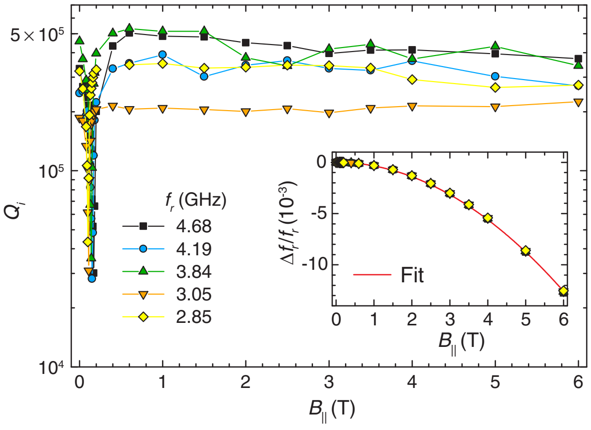

FIG. 3. Evolution of nanowire resonator characteristics with an in-plane magnetic field $B_\parallel$ ($w = 100$ nm, $T = 280$ mK, $P_{\mathrm{in}} \approx -110$ dBm). The intrinsic quality factor Q_i remains unaffected in the range 400 mT $\lesssim B_\parallel \le 6$ T. The maximum $B_\parallel$ is limited by our experimental setup. (Inset) All fractional frequency shifts fit to the same simple quadratic curve.

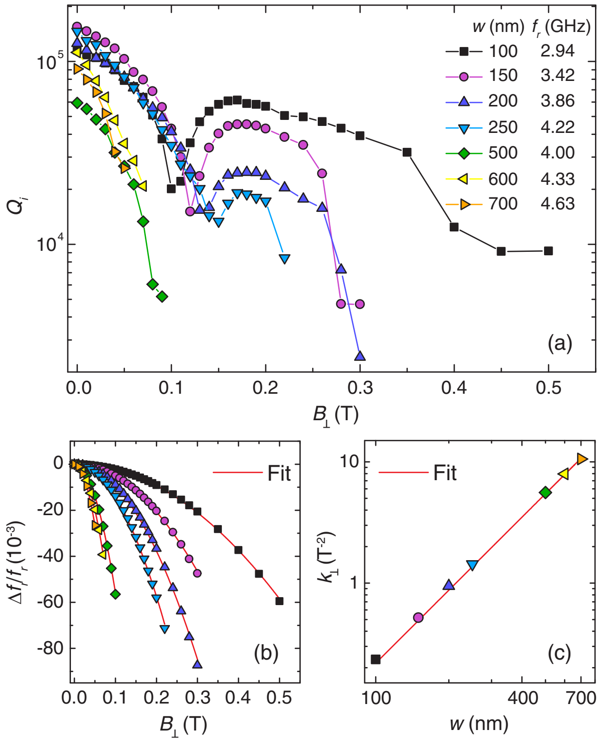

FIG. 4. Evolution of nanowire resonator characteristics with a perpendicular magnetic field, $B_\perp$. (a) Q_i as a function of $B_\perp$ for various nanowire widths w. The dips in Q_i at low field suggest coupling to magnetic impurities, similar to the case for $B_\parallel$ in Fig. 2. The narrowest resonator retains $Q_i > 3 \times 10^4$ up to $B_\perp = 350$ mT. (b) Fractional shift of the resonance frequencies with $B_\perp$. Same symbols as in (a). The red curves are best fits of $\Delta f_r/f_r = -k_\perp(w)B_\perp^2$ to the data. (c) Best-fit coefficient $k_\perp$ versus w and best quadratic fit.

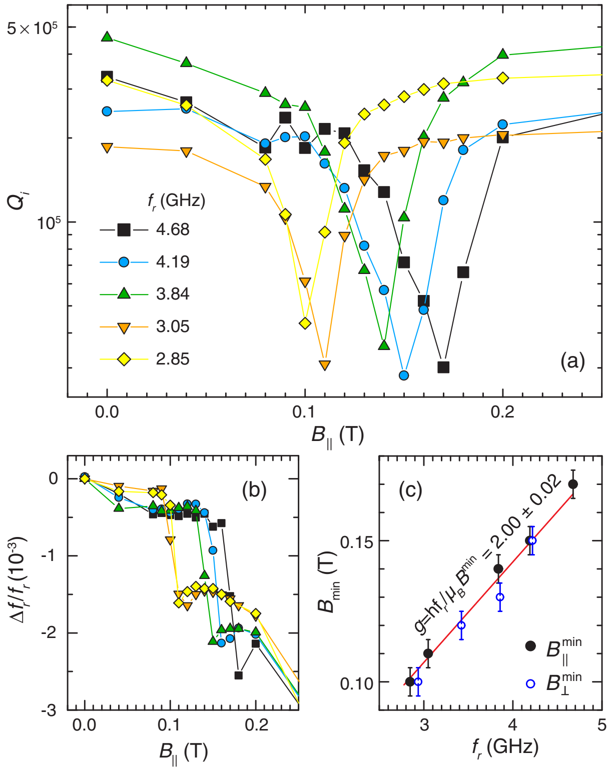

FIG. 5. Signatures of electron-spin resonance near the Zeeman field for five nanowire resonators. (a),(b) Data from Fig. 3, expanded for clarity around 100 mT. The minima of the quality factors of the resonators occur at different values of the magnetic field. (c) Dependence of the magnetic field positions of quality factor minima on the resonator frequencies. Black points correspond to $B_{\parallel}$ measurements [Fig. 3(a)], and blue points to $B_{\perp}$ measurements [Fig. 4(a)]. The straight line is the best fit to the data.

of magnitude higher than the highest at which $Q_i \approx 10^4$ has been previously reported [22].

Figures 3 and 4 show sharp dips in the quality factors of the resonators around $B_{\parallel,\perp} = 100$ mT. Upon closer inspection, it is evident that the magnetic field values, at which these dips occur, scale with the frequency of the resonators [Figs. 5(a) and 5(c)]. This suggests that the resonators couple with magnetic impurities in the silicon substrate or at one of the interfaces. Moreover, the magnetic field dependence of the frequency shifts of the resonators shows an incipient avoided crossing [Fig. 5(b)]. Fitting the frequency dependence of the magnetic field positions of the quality factor minima with the condition for spin resonance $hf_r = g\mu_B B$, we extract the value for the Landé g factor: $g = 2.00 \pm 0.02$ [Fig. 5(c)].

B. Resonance frequency shift in a magnetic field

Turning our attention to the shift of resonance frequency induced by the magnetic field, we observe for both field orientations a quadratic shift of the resonance frequency with applied field [Fig. 3 inset and Fig. 4(b)]. Fitting the fractional shifts with the expression $\Delta f_r/f_r = -k_{\parallel(\perp)} B^2_{\parallel(\perp)}$, we extract the coefficients $k_{\parallel}$ and a width-dependent $k_{\perp}(w)$ [35,36]. These coefficients reflect the increase in kinetic inductance of the superconducting nanowire due to the Cooper-pair-breaking effect of the external magnetic field. Taking into account that the dominant contribution to the nanowire inductance is kinetic, we have $f_r \propto L_k^{-1/2}$, where L_k is the kinetic inductance of the resonator. Further, for $T \ll T_c$ we have $L_k \propto T_c^{-1}$ [29], and for small changes in frequency $\Delta f_r/f_r = -\frac{1}{2}\Delta L_k/L_k = \frac{1}{2}\Delta T_C/T_C$.

The applied magnetic field splits the time-reversal degeneracy of the paired electrons, giving rise to an effective depairing energy 2α [37]. In the dirty limit and for small α, the change in T_c due to this pair-breaking effect is linear in α: $k_B \Delta T_c = -(\pi/4)\alpha$. The penetration depth in the films $\Lambda = 2\lambda^2/t \approx 50$ μm, where λ is the London penetration depth, is much greater than w. Therefore, we make use of the expression for α valid in the “thin film in parallel field” approximation, $\alpha = \frac{1}{6}(De^2 B_{\perp}^2 w^2/\hbar)$, where D is the electronic diffusion constant [37]. Thus, we recover the experimentally observed scaling $\Delta f_r/f_r = -(\pi/48)[De^2/(\hbar k_B T_c)]B_{\perp}^2 w^2$ and extract the diffusion constant $D \approx 2$ cm^2 s^{-1}. This value is consistent with an earlier estimate [38] of the electronic diffusion constant in NbTiN thin films.

Furthermore, extending this geometrical scaling to the case of a parallel field yields an effective thickness of the superconductor $t_{\mathrm{eff}} \approx 3.5$ nm. The reduced effective thickness of the film in the context of a magnetic field expulsion is likely a combined effect of surface oxidation and the suppression of shielding currents within a coherence length from the edge.

IV. SUMMARY

In summary, microwave resonators based on NbTiN nanowires with extremely small cross section are highly insensitive to a parallel magnetic field, with Q_i remaining unaffected up to $B_{\parallel} = 6$ T. Because of the high kinetic inductance of the nanowires, the resonators are expected to produce an order of magnitude higher vacuum voltage fluctuations compared to standard CPW resonators. Our next experiments will focus on achieving strong coupling between these nanowire resonators and spin qubits in gate-defined quantum dots, which have small electric dipole moments and require a magnetic field.

ACKNOWLEDGMENTS

We thank L. P. Kouwenhoven and his team for sputtering of NbTiN thin films and G. de Lange, T. M. Klapwijk, and A. Wallraff for fruitful discussions. We acknowledge funding by an ERC Synergy Grant, the Dutch Organization for Fundamental Research on Matter, the Army Research Office (Grant No. W911NF-12-0607), a Marie-Curie Career Integration Grant (L. D. C.), and Microsoft Corporation Station Q.

APPENDIX A: STUDY OF THE FUNDAMENTAL MODE

For the fundamental mode of the nanowire resonator, the voltages at the two ends of the nanowire oscillate out of phase. In order to increase the coupling of the fundamental mode to the feedline, we rotate the resonator by 90° [Figs. 6(a)–6(c)]. This enhances the capacitive coupling component of the fundamental mode of the resonator to the feedline. Figure 6(d) shows the dependence of the fundamental frequencies of five nanowire resonators ($w = 100$ nm) on the inverse of their total length, l. The linear dependence of the resonance frequencies on $1/l$ is consistent with the nanowire resonators being distributed half-wave resonators with negligible direct capacitance between the nanowire ends. To further test this hypothesis, we fabricate two of the five resonators in an open geometry [Fig. 6(c) and crosses in Fig. 6(d)] with the ends facing outwards. We find the resonance frequencies to be independent of the nanowire winding.

The thickness of the NbTiN film used in the fabrication of the new sample is approximately 6.5 nm, and it is deposited a few months after the film used in the main text. Based on Sonnet simulations of the resonance frequencies [as in Fig. 6(d)], we estimate $L_S \approx 75$ pH/□ for the new film. This value is a factor of 2 higher than that of the film used in the main text, suggesting higher degree of disorder.

Figure 6(e) shows the performance of these resonators as a function of the parallel magnetic field at $P_{\mathrm{in}} \approx -110$ dBm. At $B_{\parallel} = 0$, the intrinsic quality factors are lower than those shown in Figs. 2 and 3. However, as the magnetic field is applied, the quality factors are enhanced and by $B_{\parallel} \sim 2$ T become comparable to those reported in the main text.

APPENDIX B: RESONATOR WIDTH DEPENDENCE OF THE PERFORMANCE IN A PARALLEL MAGNETIC FIELD

Figure 7 shows the $B_{\parallel}$ evolution of Q_i and f_r for the four resonators from Fig. 4 with narrowest nanowires. The fractional frequency shifts for all resonators follow the same curve, demonstrating that the contribution from any out-of plane component due to field misalignment is negligible.

APPENDIX C: ZERO-POINT VOLTAGE FLUCTUATIONS AT THE ENDS OF THE NANOWIRE RESONATOR

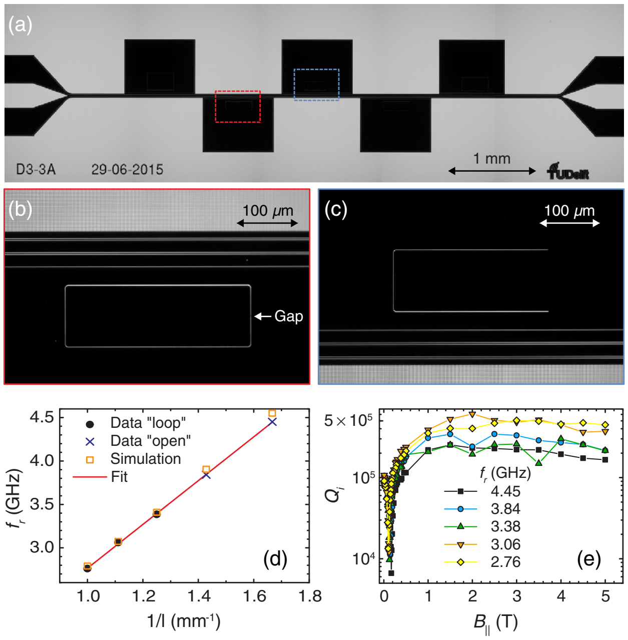

FIG. 6. (a) Dark-field micrograph of a typical device with five nanowire resonators. (b),(c) Expanded regions from (a) showing two nanowire resonators with "loop" (b) and "open" (c) geometries, respectively. Unlike the resonators shown in the main text, the fundamental modes of these resonators couple mainly capacitively to the feedline. (d) Linear dependence of the fundamental frequency of nanowire resonators ($w = 100$ nm) on the inverse of their length, l. Frequencies are independent of how the nanowire winds. (e) Evolution of the intrinsic quality factor of the fundamental modes with $B_{\parallel}$.

Figure 6 demonstrates that the nanowire resonator acts as a distributed half-wavelength resonator. Thus, in the lowest mode, current distribution on the resonator can be expressed as

$$I(x,t) = I_0 \sin\left(\frac{x}{l}\pi\right) \sin(\omega t), \qquad \text{(C1)}$$

where l is the length of the wire. The voltage difference over a small wire segment of length dx a distance x from the end is given by

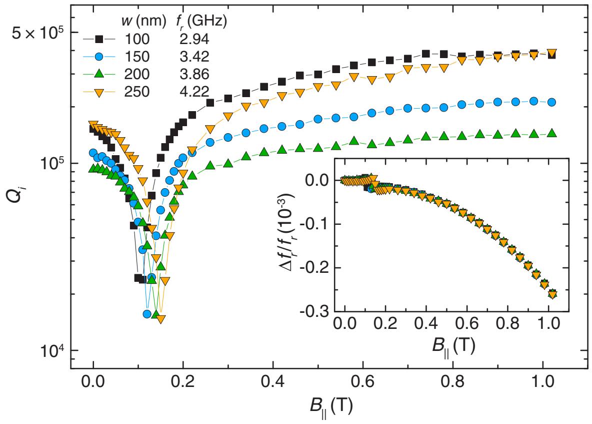

FIG. 7. $B_{\parallel}$ evolution of Q_i in the four narrowest nanowire resonators shown on Fig. 4. (Inset) Fractional shifts of the four resonance frequencies as a function of the applied field. Symbols correspond to those in the main figure.

$$dV_x = \mathcal{L}dx\frac{\partial I(x,t)}{\partial t}, \tag{C2}$$

where $\mathcal{L}$ is inductance per unit length. Plugging in the expression for $I(x,t)$ from Eq. (C1) into Eq. (C2) gives

$$dV_x = \mathcal{L}dxI_0 \sin\left(\frac{x}{l}\pi\right)\omega\cos(\omega t). \tag{C3}$$

Integrating the voltage from Eq. (C3) over the length of the wire, we arrive at the expression for the voltage difference between the two ends of the resonator:

$$\begin{aligned}\Delta V &= \mathcal{L}I_0\omega\cos(\omega t)\int_0^l \sin\left(\frac{x}{l}\pi\right)dx \\ &= \mathcal{L}I_0\omega\cos(\omega t)\frac{l}{\pi}\int_0^\pi \sin\left(\frac{x}{l}\pi\right)d\left(\frac{x}{l}\pi\right) \\ &= \mathcal{L}I_0\omega\cos(\omega t)\frac{2l}{\pi}.\end{aligned} \tag{C4}$$

Next, we estimate the amplitude of the ZPF current I_0. The average energy stored in the inductance equals half of the zero-point energy:

$$\begin{aligned}\frac{1}{4}\hbar\omega &= 1/2\frac{1}{T}\int_0^T\int_0^l \mathcal{L}I^2dxdt \\ &= 1/2\frac{I_0^2}{T}\mathcal{L}\int_0^T \sin^2(\omega t)dt\int_0^l \sin^2\left(\frac{x}{l}\pi\right) \\ &= 1/8I_0^2\mathcal{L}l.\end{aligned}$$

Therefore,

$$I_0 = \sqrt{\frac{2\hbar\omega}{\mathcal{L}l}}. \tag{C5}$$

Inserting the expression for I_0 from Eq. (C5) into Eq. (C4), we get the final expression for the voltage ZPF between two ends of the resonator:

$$\Delta V = \frac{2L}{\pi}\sqrt{\frac{2\hbar\omega}{L}}\omega\cos(\omega t).$$

Here $L = \mathcal{L}l$ is the total inductance of the resonator.

For the 4.45-GHz resonator in Fig. 6: $L_S = 75$ pH/□, $l = 600$ μm, and $w = 100$ nm. From these values, we calculate $L \approx 450$ nH and $\Delta V_{\mathrm{rms}} \approx 20$ μV.

[1] A. Blais, R.-S. Huang, A. Wallraff, S. M. Girvin, and R. J. Schoelkopf, Cavity quantum electrodynamics for superconducting electrical circuits: An architecture for quantum computation, Phys. Rev. A **69**, 062320 (2004).

[2] Z.-L. Xiang, S. Ashhab, J. Q. You, and F. Nori, Hybrid quantum circuits: Superconducting circuits interacting with other quantum systems, Rev. Mod. Phys. **85**, 623 (2013).

[3] X. Hu, Y.-x. Liu, and F. Nori, Strong coupling of a spin qubit to a superconducting stripline cavity, Phys. Rev. B **86**, 035314 (2012).

[4] G. Burkard and A. Imamoglu, Ultra-long-distance interaction between spin qubits, Phys. Rev. B **74**, 041307 (2006).

[5] L. Childress, A. S. Sørensen, and M. D. Lukin, Mesoscopic cavity quantum electrodynamics with quantum dots, Phys. Rev. A **69**, 042302 (2004).

[6] P.-Q. Jin, M. Marthaler, A. Shnirman, and G. Schön, Strong Coupling of Spin Qubits to a Transmission Line Resonator, Phys. Rev. Lett. **108**, 190506 (2012).

[7] C. Kloeffel, M. Trif, P. Stano, and D. Loss, Circuit QED with hole-spin qubits in Ge/Si nanowire quantum dots, Phys. Rev. B **88**, 241405 (2013).

[8] D. Loss and D. DiVincenzo, Quantum computation with quantum dots, Phys. Rev. A **57**, 120 (1998).

[9] R. Hanson, L. P. Kouwenhoven, J. R. Petta, S. Tarucha, and L. M. K. Vandersypen, Spins in few-electron quantum dots, Rev. Mod. Phys. **79**, 1217 (2007).

[10] J. T. Muhonen, J. P. Dehollain, A. Laucht, F. E. Hudson, R. Kalra, T. Sekiguchi, K. M. Itoh, D. N. Jamieson, J. C. McCallum, A. S. Dzurak, and A. Morello, Storing quantum information for 30 seconds in a nanoelectronic device, Nat. Nanotechnol. **9**, 986 (2014).

[11] K. D. Petersson, L. W. McFaul, M. D. Schroer, M. Jung, J. M. Taylor, A. A. Houck, and J. R. Petta, Circuit quantum electrodynamics with a spin qubit, Nature (London) **490**, 380 (2012).

[12] T. Frey, P. J. Leek, M. Beck, A. Blais, T. Ihn, K. Ensslin, and A. Wallraff, Dipole Coupling of a Double Quantum Dot to a Microwave Resonator, Phys. Rev. Lett. **108**, 046807 (2012).

[13] J. J. Viennot, M. C. Dartiailh, A. Cottet, and T. Kontos, Coherent coupling of a single spin to microwave cavity photons, Science **349**, 408 (2015).

[14] G.-W. Deng, D. Wei, J. R. Johansson, M.-L. Zhang, S.-X. Li, H.-O. Li, G. Cao, M. Xiao, T. Tu, G.-C. Guo, H.-W. Jiang, F. Nori, and G.-P. Guo, Charge Number Dependence of the Dephasing Rates of a Graphene Double Quantum Dot in a Circuit QED Architecture, Phys. Rev. Lett. **115**, 126804 (2015).

[15] A. Megrant, C. Neill, R. Barends, B. Chiaro, Y. Chen, L. Feigl, J. Kelly, E. Lucero, M. Mariantoni, P. J. J. O'Malley, D. Sank, A. Vainsencher, J. Wenner, T. C. White, Y. Yin, J. Zhao, C. J. Palmstrøm, J. M. Martinis, and A. N. Cleland, Planar superconducting resonators with internal quality factors above one million, Appl. Phys. Lett. **100**, 113510 (2012).

[16] A. Bruno, G. de Lange, S. Asaad, K. L. van der Enden, N. K. Langford, and L. DiCarlo, Reducing intrinsic loss in superconducting resonators by surface treatment and deep etching of silicon substrates, Appl. Phys. Lett. **106**, 182601 (2015).

[17] R. Wördenweber, P. Dymashevski, and V. R. Misko, Guidance of vortices and the vortex ratchet effect in high-T_c superconducting thin films obtained by arrangement of antidots, Phys. Rev. B **69**, 184504 (2004).

[18] C. Song, T. W. Heitmann, M. P. DeFeo, K. Yu, R. McDermott, M. Neeley, J. M. Martinis, and B. L. T. Plourde, Microwave response of vortices in superconducting thin films of Re and Al, Phys. Rev. B **79**, 174512 (2009).

[19] D. Bothner, C. Clauss, E. Koroknay, M. Kemmler, T. Gaber, M. Jetter, M. Scheffler, P. Michler, M. Dressel, D. Koelle, and R. Kleiner, Reducing vortex losses in superconducting microwave resonators with microsphere patterned antidot arrays, Appl. Phys. Lett. **100**, 012601 (2012).

[20] D. Bothner, T. Gaber, M. Kemmler, D. Koelle, and R. Kleiner, Improving the performance of superconducting microwave resonators in magnetic fields, Appl. Phys. Lett. **98**, 102504 (2011).

[21] J. I. Vestgården, V. V. Yurchenko, R. Wördenweber, and T. H. Johansen, Mechanism for flux guidance by micrometric antidot arrays in superconducting films, Phys. Rev. B **85**, 014516 (2012).

[22] S. E. de Graaf, A. V. Danilov, A. Adamyan, T. Bauch, and S. E. Kubatkin, Magnetic field resilient superconducting fractal resonators for coupling to free spins, J. Appl. Phys. **112**, 123905 (2012).

[23] S. E. de Graaf, D. Davidovikj, A. Adamyan, S. E. Kubatkin, and A. V. Danilov, Galvanically split superconducting microwave resonators for introducing internal voltage bias, Appl. Phys. Lett. **104**, 052601 (2014).

[24] A. Ghirri, C. Bonizzoni, D. Gerace, S. Sanna, A. Cassinese, and M. Affronte, $YBa_2Cu_3O_7$ microwave resonators for strong collective coupling with spin ensembles, Appl. Phys. Lett. **106**, 184101 (2015).

[25] P. K. Day, H. G. DeLuc, B. A. Mazin, A. Vayonakis, and J. Zmuidzinas, A broadband superconducting detector suitable for use in large arrays, Nature (London) **425**, 817 (2003).

[26] J. Luomahaara, V. Vesterinen, L. Grönberg, and J. Hassel, Kinetic inductance magnetometer, Nat. Commun. **5**, 4872 (2014).

[27] The NbTiN films are deposited in an ATC-180 UHV custom sputtering system from AJA International Inc., with dc-magnetron sputtering from a Nb(70%)/Ti(30%) target, in a reactive atmosphere of argon (90%) and nitrogen (10%) at pressure 3 mTorr and 250 W power. Typical values for substrate temperature and voltage bias are 20 °C and −45 V, respectively.

[28] M. S. Khalil, M. J. A. Stoutimore, F. C. Wellstood, and K. D. Osborn, An analysis method for asymmetric resonator transmission applied to superconducting devices, J. Appl. Phys. **111**, 054510 (2012).

[29] A. J. Annunziata, D. F. Santavicca, L. Frunzio, G. Catelani, M. J. Rooks, A. Frydman, and D. E. Prober, Tunable superconducting nanoinductors, Nanotechnology **21**, 445202 (2010).

[30] J. Gao, M. Daal, A. Vayonakis, S. Kumar, J. Zmuidzinas, B. Sadoulet, B. A. Mazin, P. K. Day, and H. G. Leduc, Experimental evidence for a surface distribution of two-level systems in superconducting lithographed microwave resonators, Appl. Phys. Lett. **92**, 152505 (2008).

[31] A. D. O'Connell, M. Ansmann, R. C. Bialczak, M. Hofheinz, N. Katz, E. Lucero, C. McKenney, M. Neeley, H. Wang, E. M. Weig, A. N. Cleland, and J. M. Martinis, Microwave dielectric loss at single photon energies and millikelvin temperatures, Appl. Phys. Lett. **92**, 112903 (2008).

[32] P. C. J. J. Coumou, M. R. Zuiddam, E. F. C. Driessen, P. J. de Visser, J. J. A. Baselmans, and T. M. Klapwijk, Microwave properties of superconducting atomic-layer deposited TiN films, IEEE Trans. Appl. Supercond. **23**, 7500404 (2013).

[33] V. Ranjan, G. de Lange, R. Schutjens, T. Debelhoir, J. P. Groen, D. Szombati, D. J. Thoen, T. M. Klapwijk, R. Hanson, and L. DiCarlo, Probing Dynamics of an Electron-Spin Ensemble via a Superconducting Resonator, Phys. Rev. Lett. **110**, 067004 (2013).

[34] D. I. Schuster, A. P. Sears, E. Ginossar, L. DiCarlo, L. Frunzio, J. J. L. Morton, H. Wu, G. A. D. Briggs, B. B. Buckley, D. D. Awschalom, and R. J. Schoelkopf, High-Cooperativity Coupling of Electron-Spin Ensembles to Superconducting Cavities, Phys. Rev. Lett. **105**, 140501 (2010).

[35] J. E. Healey, T. Lindstrm, M. S. Colclough, C. M. Muirhead, and A. Y. Tzalenchuk, Magnetic field tuning of coplanar waveguide resonators, Appl. Phys. Lett. **93**, 043513 (2008).

[36] D.-H. Wu, C. A. Shiffman, and S. Sridhar, Field variation of the penetration depth in ceramic $Y_1Ba_2Cu_3O_y$, Phys. Rev. B **38**, 9311 (1988).

[37] M. Tinkham, *Introduction to Superconductivity*, 2nd ed. (McGraw-Hill, New York, 1996).

[38] C. Tong, J. Stern, Megerian, H. LeDuc, T. Sridharan, H. Gibson, and R. Blundell, in A low-noise NbTiN hot electron bolometer mixer, *Proceedings of the 12th International Symposium on Space THz Technology, California, 2001* (JPL Publication, Pasadena, California, 2001), p. 253.